Integral Resonant Controller for Suppressing Car's Oscillations and Eliminating its Inherent Jump Phenomenon

Ali Kandil[1,2,*], Y. S. Hamed[3]

[1] *Department of Applied and Computational Mathematics, Institute of Basic and Applied Sciences, Egypt-Japan University of Science and Technology (E-JUST), New Borg El-Arab 21934, Alexandria, Egypt*
[2] *Department of Physics and Engineering Mathematics, Faculty of Electronic Engineering, Menoufia University, Menouf 32952, Egypt*
[3] *Department of Mathematics and Statistics, College of Science, Taif University, P. O. Box 11099, Taif 21944, Saudi Arabia*

Abstract. This work deals with modeling and controlling the oscillations of a horizontally-supported car under the effect of a nonlinear spring, a damper, and a harmonic excitation external force. The proposed controller is the integral resonant controller (IRC) which is a first order oscillator coupled the car via a linear variable differential transformer (LVDT) and a servo-controlled linear actuator (SCLA). The multiple scales perturbation method is used to obtain an approximate solution and stability analyses are carried out. Based on the stability analysis, the optimum values of the controller parameters are recommended in this work for a better control operation. Several response curves are plotted for clarifying the concept of the proposed integral resonant control algorithm. A numerical simulation of the car's motion is achieved by numerically integrating the model equations with the 4th order Rung-Kutta algorithm. The applied controller can treat the severe jumps in the oscillation amplitude where it is suppressed at different conditions of forward and backward sweeping of the amplitude and frequency of the external excitation force.

2020 Mathematics Subject Classifications: 34A34, 34C15, 34C23, 34C25, 34D20, 34E13, 37N15, 70B05, 70K05, 70K40, 70K42, 70K50

Key Words and Phrases: Multiple scales perturbation technique, Integral resonant controller, Jump phenomenon, Stability analysis, Mass-Damper-Spring

1. Introduction

Vibration control of mechanical systems has become the focus of many researchers all over the world. Different techniques have been applied and investigated in order to

---

reach a safe system operation with less defects and costs. Some of them depends on passive control where bulky elements are used without any adaptation to the change in the system states. The other type relies on active control where a control equation (algorithm) is programmed into a control unit that gets the feedback signals from the system states then acts upon their values. Among these active control techniques is the integral resonant controller (IRC) that is a first order oscillator coupled linearly to the controlled model equation. In addition, one of the most important models to be controlled is the car model that suffers from unwanted oscillations. Aphale et al. [2] proposed the IRC for controlling a smart structure implanted with distributed sensors and actuators. They showed that applying such controller resulted in better operation and stability. Díaz and Reynolds [6] designed a robust proof-mass actuator in order to suppress the induced vibrations by humans in floor structures. This actuator influenced the system dynamics by inserting a feed-through term to the system acceleration output. Ji and Zhang [11] explored the hysteresis and jump phenomena that could occur in the equilibrium response of a simple mass-damper-spring absorber connected to a half-car model excited harmonically. Febbo [7] discussed the nonlinear dynamics of an extensible oscillator that was driven harmonically with the aid of the harmonic balance method for extracting the frequency response equations. Pereira et al. [27] proposed an IRC technique composed of an inner loop to control a joint-angle, and an outer loop to suppress the unwanted vibrations of the joint. Díaz et al. [5] introduced a simple and robust technique for mitigating the vibrations of smart structures implanted with sensor-actuator pairs where the closed-loop system produced high stability margins. Ji [10] controlled the primary resonance of a nonlinear oscillator with the help of a nonlinear vibration absorber where the natural frequencies of both the oscillator and the absorber were not in an internal resonance condition. Al-Mamun et al. [1] applied a notch filter in cascade with a micro-actuator (with the idea of IRC) in order to attenuate the high resonant vibrations of the studied actuator. Febbo and Ji [8] adopted the use of Lagrange multipliers in order to find the critical forcing amplitude where a nonlinear oscillator exhibited hysteresis and jump phenomena in the primary resonance case. Liu et al. [16] introduced a feedback control with time-delay for reducing the primary resonant vibrations of a carbon nanotube excited by a Lorentz force and a longitudinal magnetic field. Omidi and Mahmoodi [24] have combined the algorithms of positive position feedback (PPF) controller and IRC in order to overcome some issues that were raised in the PPF controller. They adopted the method of multiple scales for extracting the modulation equations of the amplitude and phase of the studied system's oscillations. Xu and Sun [31] studied the effect of the multi directional quasi-zero-stiffness isolator that was coupled to a time delayed linear active controller. Liu et al. [17] developed an optimal time delayed feedback controller for reducing the primary and secondary (super harmonic) resonances of a simply supported beam implanted with piezoelectric actuator and sensor where the stability regions were plotted depending on the eigenvalue equation. Omidi and Mahmoodi [25] introduced a nonlinear form of the IRC in order to suppress the vibratory behavior of some smart structures where an extra damping was added to the closed-loop system. Ozer et al. [26] suggested a novel fuzzy-logic controller for suppressing the buildings vibrations that consisted of steel plates and

columns with an optimal mass dynamic absorber. Liu et al. [21] investigated the effect of a dynamic vibration absorber on reducing the oscillations of a prism where linear damping and stiffness and elastic foundation were considered. Bronkhorst et al. [4] identified an SDOF (single degree-of-freedom) cubic-nonlinearity model whose vibrations were reduced via a viscoelastic dynamic absorber. Liu et al. [18, 19] proposed different kinds of time-delayed proportional-derivative active controllers in order to mitigate the oscillations in a cantilever beam once with a lumped mass and another with an axial load. Kandil et al. [14] proposed the control of a mass-damper-spring model with the aid of servo-controlled linear actuator and linear variable differential transformer as a sensor where the control signal was proportional to the mass position. Zhou et al. [34] studied the effect of moving the base of a magnetically coupled oscillator on the dynamical behavior of the saturated equilibrium response. Bauomy and Taha [3] coupled a primary system (cantilever beam) to a secondary system (nonlinear vibration absorber) under the effect of a harmonic excitation force in order to reduce the beam's vibrations. Xu et al. [32] evaluated the designs of H_2 and H_∞ techniques with tuned inerter damper (TID) on the damped structures in order to obtain the frequency response function of the equipped system with TIDs. Wang et al. [30] proposed a meta-structure of low-frequency multi-layers for reducing the broadband vibrations where the time delay effect was studied as well. Kandil et al. [12, 13, 15] suggested different techniques for controlling the vibrations of a half-car model in case of primary, super-harmonic, and sub-harmonic resonance cases. They applied the well-known nonlinear saturation controller and a new cubic-position-negative-velocity feedback controller for the mentioned resonance cases. Liu et al. [20] combined a graphene sheet of a single layer resting on a visco-Pasternak foundation excited by a dual-frequency force where a time-delayed proportional-derivative controller was applied for the first time. Saeed et al. [28] utilized the IRC technique for reducing the lateral (horizontal and vertical) oscillations of the rotor active magnetic bearings system for the first time. Geng et al. [9] limited the high oscillations of a nonlinear energy sink by improving its reliability with a contactless magnetic force where the dynamical characteristics were analyzed via analytical and numerical approaches. Mohanty and Dwivedy [22] proposed a non-traditional nonlinear absorber in order to suppress the oscillations of a base-excited nonlinear mass-spring model excited by hard external and parametric forces. Zhang et al. [33] mixed a nonlinear energy sink with an internal oscillator to control the vibrations of laminated composite plates where the efficiency of that mix is better in frequency responses and energy dissipation. This work introduces the modeling of a horizontally-supported car's motion under the effect of a nonlinear spring, a damper, and a harmonic excitation external force. The car's oscillations can be controlled via an integral resonant controller whose operation is fulfilled via a linear variable differential transformer and a servo-controlled linear actuator. The multiple scales perturbation technique is adopted to seek an approximate solution of the proposed nonlinear system of equations. In addition, a stability analysis is achieved in order to determine whether the extracted approximate solution is stable or not. Several response curves are plotted for clarifying the concept of the proposed control algorithm. We discuss this problem from a mathematical background with stating all the assumptions clearly in the paper. We know that it may be far from

the actual automobile system. But we want to say that the IR controller may have a vibration suppression effect on the model's oscillations based on mathematical proof. In the future, we are going to enroll automobile real-life simulations from licensed software to simulate such automobile motions under the proposed control.

2. Car's Motion Dynamical Equation and Its Approximate Solution

Figure 1a shows a car (of mass m) which is horizontally-supported with a nonlinear spring of stiffness C_1 and C_2 and a damper of viscosity factor C. The car is also excited by an unwanted harmonic force $f \cos(\Omega t)$ that causes the car exhibit undesired horizontal oscillations $x(t)$. These oscillations are to be controlled via the control unit that is detailed in Fig. 1b.
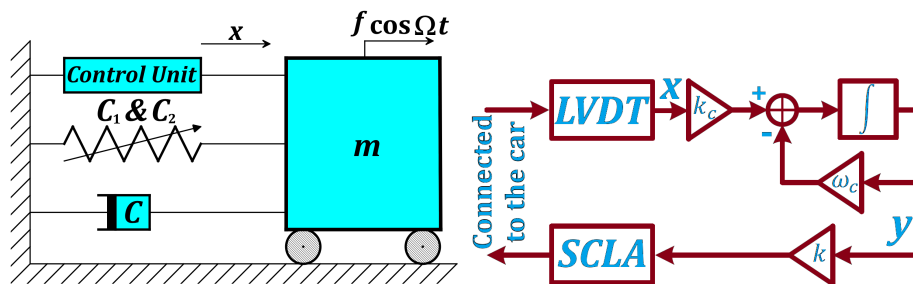

Figure 1: (left) Horizontally-supported car connected to a control unit, (right) detailed control unit

Herein, the external forces are the harmonic force $f \cos(\Omega t)$ and the control unit force $F_c(t)$, while the only dissipative force is the damper's force which opposes the motion direction, i.e. $-Cv$ or $-C\dot{x}$. Using all of these quantities leads to the following equation of motion

$$m\ddot{x} + C\dot{x} + C_1 x + C_2 x^3 = f \cos(\Omega t) + F_c(t) \tag{1}$$

In this work, we are controlling the car's oscillations with an integral resonant controller (IRC) that has the form [24, 25, 28]

$$\dot{y} + \omega_c y = k_c x \tag{2}$$

where ω_c is the decay rate of natural response of $y(t)$ and k_c is the feedback gain. This type of first order oscillator can be implemented as shown in Fig. 1b. Its input feedback signal $x(t)$ is acquired from a linear variable differential transformer (LVDT), while its output control signal is applied to a servo-controlled linear actuator (SCLA). The LVDT and SCLA devices are connected directly to the car for sensing and actuating purposes, respectively. For the oscillator's equation shown in Eq. (2), it should be coupled linearly with Eq. (1). Hence, the control force should be in the form $F_c = ky$ where k is the control gain. Using this data with simplifying Eq. (1), we have a system of differential equations as follows

$$\ddot{x} + \mu\dot{x} + \omega^2 x + \alpha x^3 = \hat{f}\cos(\Omega t) + \hat{k}y \tag{3}$$

$$\dot{y} + \omega_c y = k_c x \tag{4}$$

where $\mu = C/m$, $\omega^2 = C_1/m$, $\alpha = C_2/m$, $\hat{f} = f/m$, $\hat{k} = k/m$. For brevity, we will remove the hats in the next analysis. A suitable scaling is done for some parameters such that $\mu = \epsilon\tilde{\mu}$, $\alpha = \epsilon\tilde{\alpha}$, $f = \epsilon\tilde{f}$, and $k_c = \epsilon\tilde{k}_c$ in order to show the perturbed problem rather than the linear un-damped free problem [23]. The tildes are used to show that the parameters are scaled, while ϵ is a small perturbation parameter. Equations (3) and (4) become

$$\ddot{x} + \epsilon\tilde{\mu}\dot{x} + \omega^2 x + \epsilon\tilde{\alpha}x^3 = \epsilon\tilde{f}\cos(\Omega t) + ky \tag{5}$$

$$\dot{y} + \omega_c y = \epsilon\tilde{k}_c x \tag{6}$$

The approximate solution of the system above is sought with asymptotic series [23] as follows

$$x(t) = \sum_{n=0}^{\infty} \epsilon^n x_n \approx x_0 + \epsilon x_1 \tag{7}$$

$$y(t) = \sum_{n=0}^{\infty} \epsilon^{n+1} y_n \approx \epsilon y_0 + \epsilon^2 y_1 \tag{8}$$

where x_n and y_n are the component functions comprising the main solutions. The time-derivatives can also be approximated by new partials derivatives in terms of new time scales $T_0 = t$ and $T_1 = \epsilon t$ as follows:

$$\frac{d}{dt} = \sum_{n=0}^{\infty} \epsilon^n \frac{\partial}{\partial T_n} \approx \frac{\partial}{\partial T_0} + \epsilon\frac{\partial}{\partial T_1} \tag{9}$$

Substituting Eqs. (7) to (9) into Eqs. (5) and (6) and extracting the terms of equal powers of ϵ (up to ϵ^1) on both sides lead us to the following:

$$\frac{\partial^2 x_0}{\partial T_0^2} + \omega^2 x_0 = 0 \tag{10}$$

$$\frac{\partial y_0}{\partial T_0} + \omega_c y_0 = \tilde{k}_c x_0 \tag{11}$$

$$\frac{\partial^2 x_1}{\partial T_0^2} + \omega^2 x_1 = -2\frac{\partial^2 x_0}{\partial T_0 \partial T_1} - \tilde{\mu}\frac{\partial x_0}{\partial T_0} - \tilde{\alpha}x_0^3 + \frac{\tilde{f}}{2}(e^{i\Omega T_0} + e^{-i\Omega T_0}) + ky_0 \tag{12}$$

Equation (10) has the basic solution of a simple harmonic motion problem such that

$$x_0 = Ae^{i\omega T_0} + \bar{A}e^{-i\omega T_0} \tag{13}$$

where A and its conjugate $\bar{A}$ are unknown quantities in terms of T_1. Substituting x_0 from Eq. (13) into Eq. (11), then solving the resulting first order differential equation lead us to

$$y_0 = Be^{-\omega_c T_0} + \tilde{\Gamma}Ae^{i\omega T_0} + \bar{\tilde{\Gamma}}\bar{A}e^{i\omega T_0} \tag{14}$$

where B is another unknown quantity in terms of T_1 and $\tilde{\Gamma} = \tilde{k}_c(\omega_c - i\omega)(\omega_c^2 + \omega^2)^{-1}$. Substituting Eqs. (13) and (14) into Eq. (12) yields

$$\frac{\partial^2 x_1}{\partial T_0^2} + \omega^2 x_1 = (-2i\omega\frac{\partial A}{\partial T_1} - i\tilde{\mu}\omega A - 3\tilde{\alpha}A^2\bar{A} + \tilde{\Gamma}A)e^{i\omega T_0} + \frac{\tilde{f}}{2}e^{i\Omega T_0} + NST + c.c. \quad (15)$$

where NST stands for the non-secular terms that have no small divisors, and $c.c.$ stands for the complex conjugate of the whole preceding terms. We consider the primary resonance case at which $\Omega - \omega = \sigma$ where σ is the deviation between the excitation frequency Ω and the car's motion natural frequency ω. Assuming this deviation into Eq. (15) in order to get the overall solvability condition

$$-2i\omega\frac{\partial A}{\partial T_1} - i\tilde{\mu}\omega A - 3\tilde{\alpha}A^2\bar{A} + \tilde{\Gamma}A + \frac{\tilde{f}}{2}e^{i\sigma T_0} = 0 \quad (16)$$

Based on Eq. (9) and the fact that A is a function of T_1 only, we have

$$\dot{A} = \frac{dA}{dt} = \epsilon\frac{\partial A}{\partial T_1} \quad (17)$$

Using Eq. (17) and the assumption that $\mu = \epsilon\tilde{\mu}$, $\alpha = \epsilon\tilde{\alpha}$, $f = \epsilon\tilde{f}$, and $k_c = \epsilon\tilde{k}_c$, one can convert Eq. (16) to be in terms of t only as follows

$$-2i\omega\dot{A} - i\mu\omega A - 3\alpha A^2\bar{A} + \Gamma A + \frac{f}{2}e^{i\sigma t} = 0 \quad (18)$$

The quantities A, $\bar{A}$, and $\dot{A}$ can be expressed in polar form in order to get the amplitude and phase of the car's motion as follows

$$A = \frac{1}{2}ae^{i\delta} \quad (19)$$

$$\bar{A} = \frac{1}{2}ae^{-i\delta} \quad (20)$$

$$\dot{A} = \frac{1}{2}(\dot{a}e^{i\delta} + ia\dot{\delta}e^{i\delta}) \quad (21)$$

where $a(t)$ and $\delta(t)$ are the temporal amplitude and phase of the car's motion, respectively. Substituting Eqs. (19) to (21) into Eqs. (18) with separating the real and imaginary parts lead to

$$\dot{a} = -\frac{1}{2}\left(\mu + \frac{kk_c}{\omega_c^2 + \omega^2}\right)a + \frac{f}{2\omega}\sin(\sigma t - \delta) \quad (22)$$

$$a\dot{\delta} = -\frac{kk_c\omega_c}{2\omega(\omega_c^2 + \omega^2)}a + \frac{3\alpha}{8\omega}a^3 - \frac{f}{2\omega}\cos(\sigma t - \delta) \quad (23)$$

To convert the non-autonomous system in Eqs. (22) and (23) to an autonomous one, we should propose a new variable ψ satisfying $\psi = \sigma t - \delta$. This can give us the following autonomous system

$$\dot{a} = -\frac{1}{2}\left(\mu + \frac{kk_c}{\omega_c^2 + \omega^2}\right)a + \frac{f}{2\omega}\sin\psi \quad (24)$$

$$a\dot{\psi} = \left(\sigma + \frac{kk_c\omega_c}{2\omega(\omega_c^2 + \omega^2)}\right)a - \frac{3\alpha}{8\omega}a^3 + \frac{f}{2\omega}\cos\psi \tag{25}$$

We can see that the original damping parameter μ is enhanced by a new quantity $\mu_c = kk_c/(\omega_c^2 + \omega^2)$, while the original detuning parameter σ is enhanced by a new quantity $\sigma_c = kk_c\omega_c/2\omega(\omega_c^2 + \omega^2)$. Considering the steady-state relations such that $\dot{a} = \dot{\psi} = 0$ directs us to

$$(\mu + \mu_c)a_{ss} = \frac{f}{\omega}\sin\psi_{ss} \tag{26}$$

$$-2(\sigma + \sigma_c)a_{ss} + \frac{3\alpha}{4\omega}a_{ss}^3 = \frac{f}{\omega}\cos\psi_{ss} \tag{27}$$

where a_{ss} and ψ_{ss} represent the steady-state amplitude and phase of the car's motion. Eliminating ψ_{ss} from Eqs. (26) and (27) yields

$$\left((\mu + \mu_c)^2 + \left(2(\sigma + \sigma_c) - \frac{3\alpha}{4\omega}a_{ss}^2\right)^2\right)a_{ss}^2 - \frac{f^2}{\omega^2} = 0 \tag{28}$$

The equation above is of sixth-degree and can represent several responses such as the frequency-response (a versus σ), the force-response (a versus f), the nonlinearity-response (a versus α), the damping-response (A versus μ), or the control-gain-response (a versus k). These response curves should be tested for stability because they might have stable or unstable branches all over the domain of the variating parameter. Hence, we can make a linearization for the system in Eqs. (24) and (25) to get a linearized system involving the Jacobian matrix of partial derivatives [23, 29] as follows

$$\begin{bmatrix} \dot{a}_{sd} \\ \dot{\psi}_{sd} \end{bmatrix} = \begin{bmatrix} -\frac{1}{2}(\mu + \mu_c) & \frac{f}{2\omega}\cos\psi_{ss} \\ -\frac{3\alpha}{4\omega}a_{ss} - \frac{f}{2\omega a_{ss}^2}\cos\psi_{ss} & -\frac{f}{2\omega a_{ss}}\sin\psi_{ss} \end{bmatrix} \begin{bmatrix} a_{sd} \\ \psi_{sd} \end{bmatrix} \tag{29}$$

where a_{sd} and ψ_{sd} represent the small-deviations around the steady-state amplitude and phase of the car's motion such that $a = a_{ss} + a_{sd}$ and $\psi = \psi_{ss} + \psi_{sd}$. The nature of the eigenvalues of the Jacobian matrix above can determine the stability of a_{ss} and ψ_{ss}. In other words, all the eigenvalues with negative real parts refer to asymptotically stable amplitude and phase. Otherwise, they are unstable. This criterion is taken into account during plotting the curves on the computer software that is programmed with such criterion.

3. Car's Motion Different Responses

Upon reaching Eq. (28) in the previous section, different response curves of the car's motion amplitude to the frequency detuning σ, the force amplitude f, and the time t. These response curves tells the reader how the IRC can affect the behavior of the car's motion. According to this discussion, the model constants adopted in its operation are as follows: $\mu = 0.02$, $\omega = 3.1623$, $\alpha = 0.8$. Any other parameters will be mentioned

consequently due to the studied response. Based on the nature of the eigenvalues of the Jacobian matrix in Eq. (29), the upcoming-plotted branches are either solid referring to stable response path, or dashed referring to unstable response path. Figure 2 clarifies the response of the car's motion amplitude a to both the frequency detuning σ and the force amplitude f in case that the controller IRC is OFF ($k = 0$). Around the region whose center is $\sigma = 0$, the amplitude begins to rise as we approach the center point at $f = 0.02$ where the curve is of linear form or single stable solid branch form. As f increases to 0.04 for example, unstable dashed branch appears as shown indicating the existence of multiple branches within the hardening region. As f increases more and more, the hardening region expands accompanied by higher amplitudes. This nonlinear phenomenon shows the dependence of the curve's hardening rate (due to hard spring) on the external force amplitude that enhances the domination of the cubic nonlinearity upon the system operation. Figure 3 pictures the response of the car's motion amplitude a to both the frequency detuning σ and the damping factor μ while the controller IRC is deactivated ($k = 0$). Here, the damping factor can be an obstacle in the way of nonlinearity domination over the system. If μ increases, it can make the hardening region more wrinkled leading to decreasing the possibility of the multiple branches existence. Continuing the discussion in Fig. 4, it shows the response of the car's motion amplitude a to both the frequency detuning σ and the nonlinearity factor α with the controller IRC being disabled ($k = 0$). It is clear at $\alpha = 0$ that the car's motion amplitude responds linearly with only a single branch of solutions. In addition, as α increases positively or negatively, the car's motion amplitude curve bends proportionally to the right (hardening effect) or to the left (softening effect), respectively. This can clarify the nonlinearity domination over the car's motion response. Figure 5 indicates the response of the car's motion amplitude a to the force amplitude f and the frequency detuning σ in case that IRC is OFF ($k = 0$). As σ increases from -0.1 to 0.0, the amplitude responds in a linear manner where there are no jumps in the curve as can be seen. After that at $\sigma = 0.05$ and more, the jump phenomena start to appear where the car faces sudden jumps at every Saddle-Node bifurcation point as shown in the figure. Moreover in Fig. 6, the car's motion amplitude a is affected by to the force amplitude f along with the damping factor μ before control. The clear thing is that the interval of the unstable branch becomes narrower if the damping factor μ is increased which gives us a hint about improving the damping performance of this system to get a better car's operation. Figures 7 and 8 assure the discussion done in Fig. 4 where the positive (negative) values of α makes the car's amplitude curve bend to the right (left) only with positive (negative) values of σ.
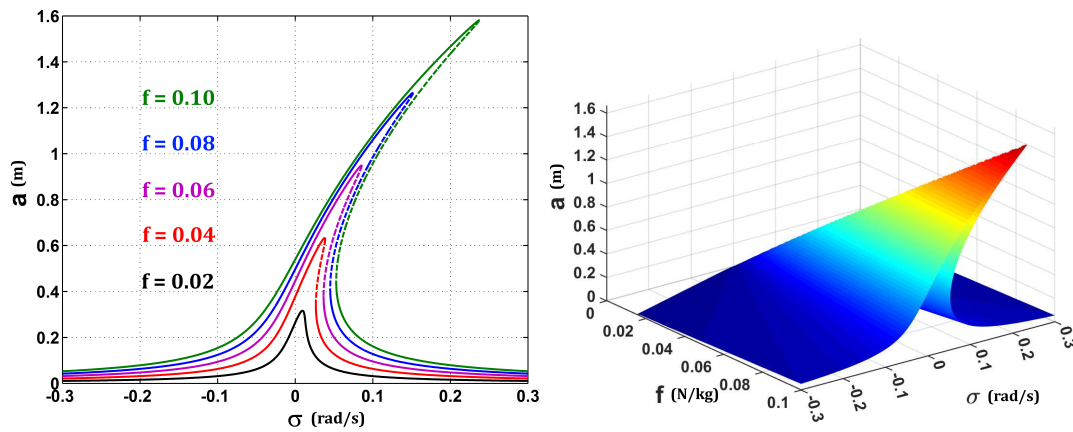
Figure 2: Response of the car's motion amplitude a to the frequency detuning σ and the force amplitude f in case that IRC is OFF ($k = 0$): (left) a versus σ at different f, (right) a versus σ and f
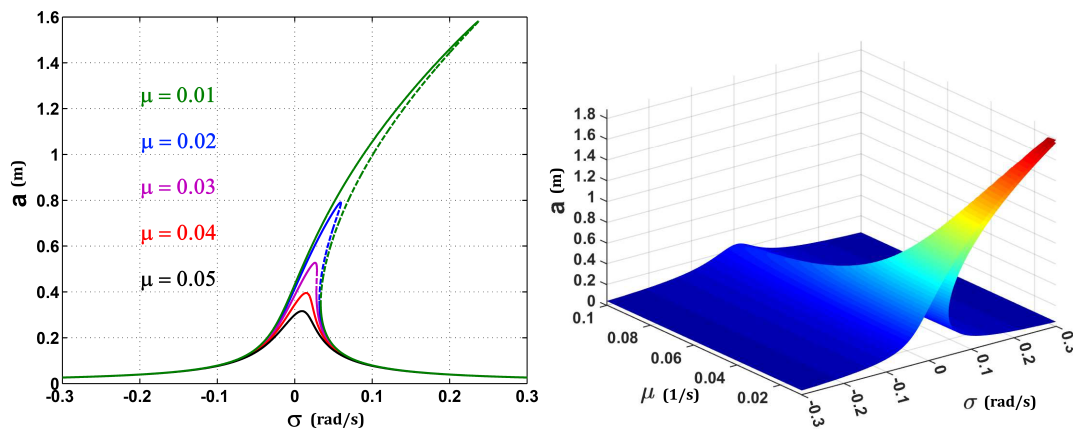

Figure 3: Response of the car's motion amplitude a to the frequency detuning σ and the damping factor μ in case that IRC is OFF ($k = 0$): (left) a versus σ at different μ, (right) a versus σ and μ
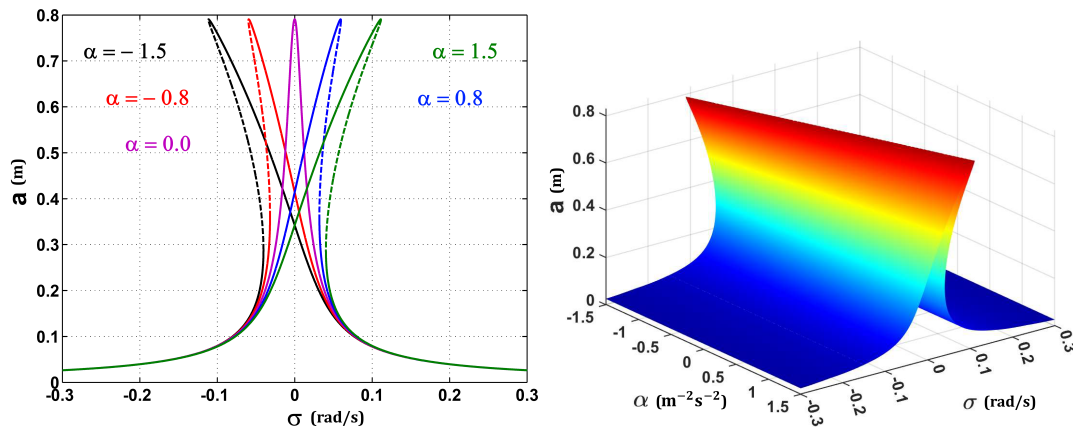
Figure 4: Response of the car's motion amplitude a to the frequency detuning σ and the nonlinearity factor α in case that IRC is OFF ($k = 0$): (left) a versus σ at different α, (right) a versus σ and α
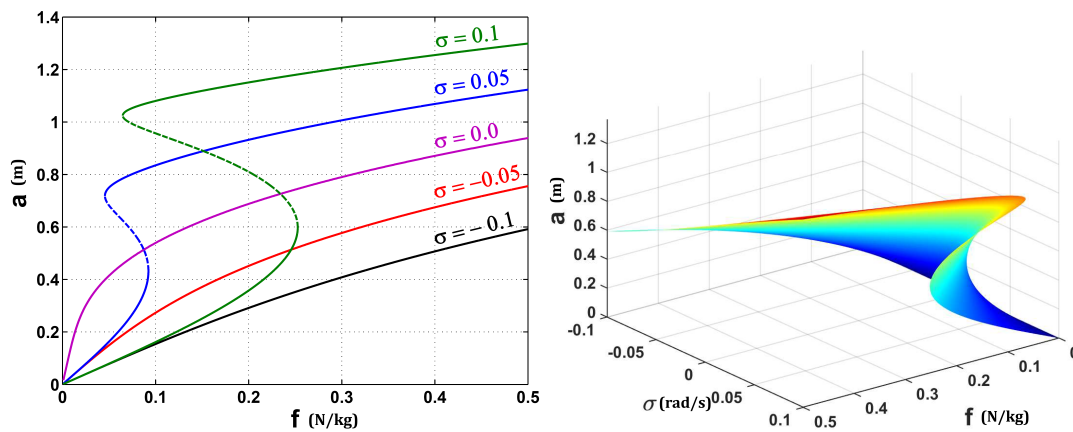

Figure 5: Response of the car's motion amplitude a to the force amplitude f and the frequency detuning σ in case that IRC is OFF ($k = 0$): (left) a versus f at different σ, (right) a versus f and σ
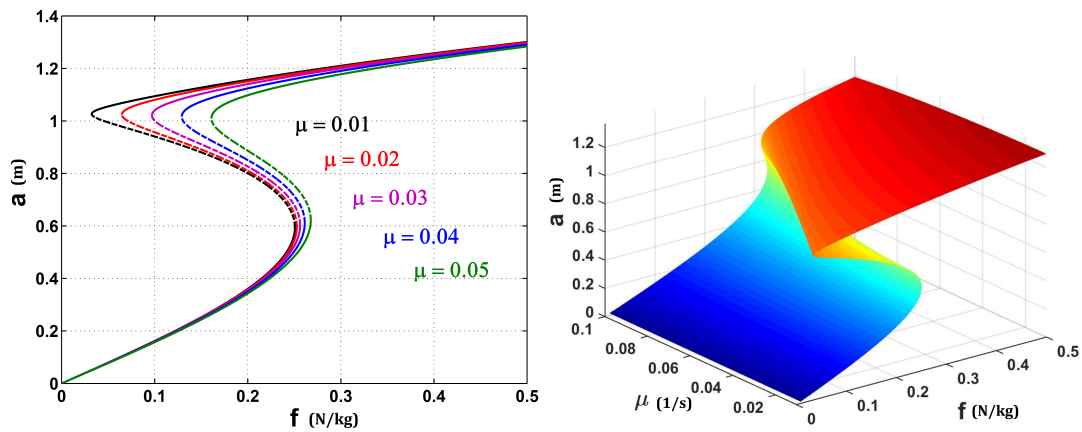
Figure 6: Response of the car's motion amplitude a to the force amplitude f and the damping factor μ in case that IRC is OFF ($k = 0$): (left) a versus f at different μ, (right) a versus f and μ
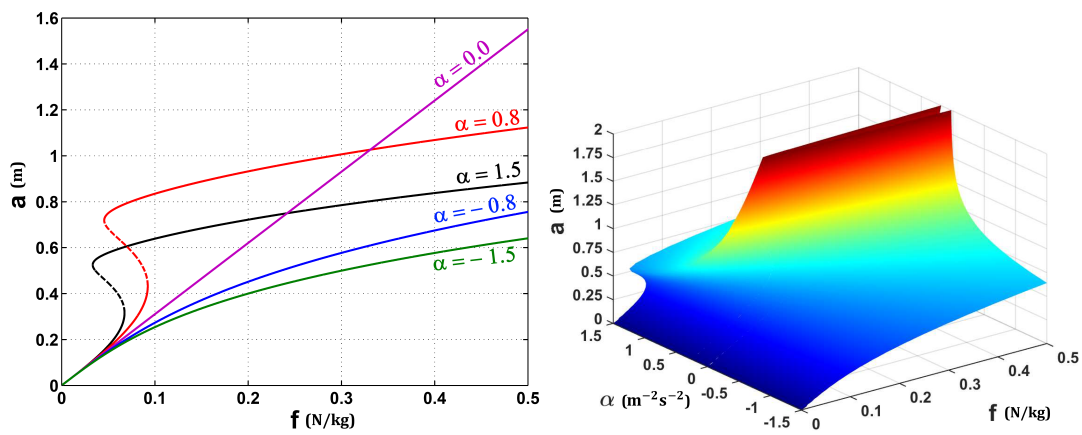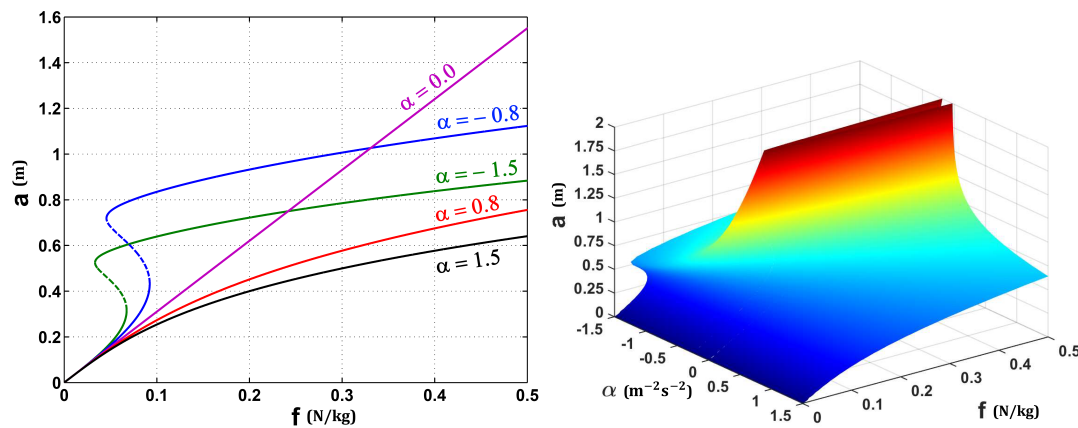

Figure 7: Response of the car's motion amplitude a to the force amplitude f and the nonlinearity factor α in case that IRC is OFF ($k = 0$ and $\sigma = 0.05$): (left) a versus f at different α, (right) a versus f and α

Figure 8: Response of the car's motion amplitude a to the force amplitude f and the nonlinearity factor α in case that IRC is OFF ($k = 0$ and $\sigma = -0.05$): (left) a versus f at different α, (right) a versus f and α

After the application of the IRC, the car's amplitude responses will be tracked in terms of the effect of the controller's parameters. We have known that the control damping factor is $\mu_c = kk_c/(\omega_c^2 + \omega^2)$ where it can be maximized either by increasing the gain product kk_c to infinity which is practically impossible, or by adjusting the control rate ω_c to be zero. The last conclusion was based upon applying the second partial derivative test on the quantity μ_c. Accordingly, Fig. 9 shows the relation of the control damping factor μ_c versus the gain product kk_c and the control rate ω_c. It is clear in Fig. 9a that the damping rate is at its maximum level only when $\omega_c = 0$ as proved by the second partial derivative test. Moreover, the damping rate decreases by increasing ω_c positively or negatively as shown. Figure 9b assures that the maximum damping rate occurs when $\omega_c = 0$ besides raising the product kk_c to 1.0 is an acceptable value for guaranteeing a better damping performance. Figure 9c combines the relation of μ_c, ω_c, and kk_c into a 3D surface as shown in order to clarify the visualization between the three parameters. On the other hand, we have that the control detuning factor is $\sigma_c = kk_c\omega_c/2\omega(\omega_c^2 + \omega^2)$. The second partial derivative test can be applied again to conclude that the factor σ_c can be maximum at $\omega_c = \pm\omega$ or it can be minimum at $\omega_c = 0$. Hence, the two quantities μ_c and σ_c can have their extreme values (maximum and minimum, respectively) by adopting the case $\omega_c = 0$ where the damping performance is at its optimum level. Accordingly, Fig. 10 indicates the relation of the control detuning factor σ_c versus the gain product kk_c and the control rate ω_c. It can be noticed that σ_c is at its lowest state and the damping rate is at its maximum level only when $\omega_c = 0$ as proved by the second partial derivative test. This is an assurance for the agreement between maximum μ_c and minimum σ_c only when $\omega_c = 0$ theoretically.
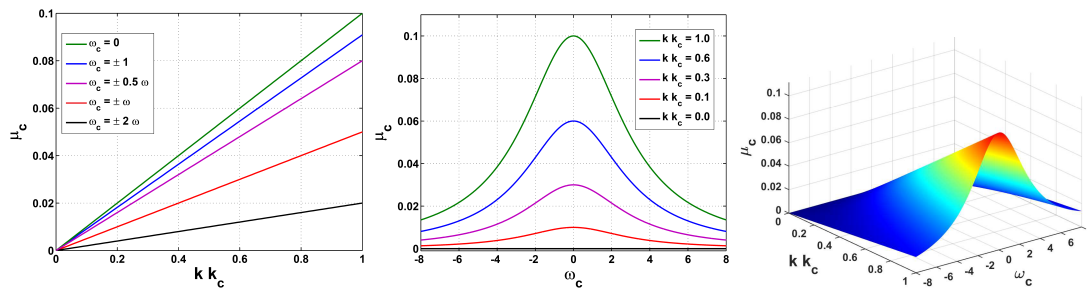
Figure 9: Relation of the control damping factor μ_c versus the gain product kk_c and the control rate ω_c: (left) μ_c versus kk_c at different ω_c, (middle) μ_c versus ω_c at different kk_c, (right) μ_c versus ω_c and kk_c
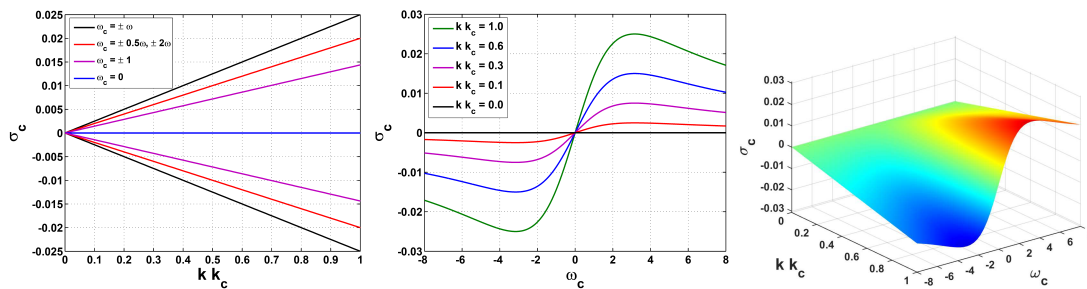
Figure 10: Relation of the control detuning factor σ_c versus the gain product kk_c and the control rate ω_c: (left) σ_c versus kk_c at different ω_c, (middle) σ_c versus ω_c at different kk_c, (right) σ_c versus ω_c and kk_c

Depending on the theoretical optimum value of ω_c, Fig. 11 is plotted to show the response of the car's motion amplitude a to the frequency detuning σ and the gain product kk_c with different values of ω_c. At $\omega_c = \omega$ in Figs. 11a and b, the amplitude is suppressed with increasing the gain product kk_c in addition to eliminating the jump phenomena that were present for lower values of kk_c. As ω_c decreases in Figs. 11c-f, the amplitude gets to better reduction ratios at $kk_c = 1.0$ ensuring that the theoretical optimum values of kk_c and ω_c are 1.0 and 0, respectively, where the oscillation amplitude has been suppressed by about 68% of its uncontrolled state at $\sigma = 0$. Figure 12 portrays the response of the car's motion amplitude a to the force amplitude f and the gain product kk_c at $\sigma = 0$ and different values of ω_c. As can be seen, the best state of the curve (lower amplitudes with respect to changing f values) is the one at $kk_c = 1.0$ and $\omega_c = 0$ in order to have better reduction ratios where the oscillation amplitude has been suppressed by about 51% of its uncontrolled state at $f = 0.1$. In addition, Fig. 13 portrays the same response as per Fig. 12 but at $\sigma = 0.1$. It is assured that the optimum curve can be reached at $kk_c = 1.0$ and $\omega_c = 0$ in order to have better reduction ratios where the oscillation amplitude has been suppressed by about 87% of its uncontrolled state at $f = 0.1$. Another aspect appears in the figure that is the elimination of the jump phenomena and the unstable region at the mentioned optimum values of kk_c and ω_c.
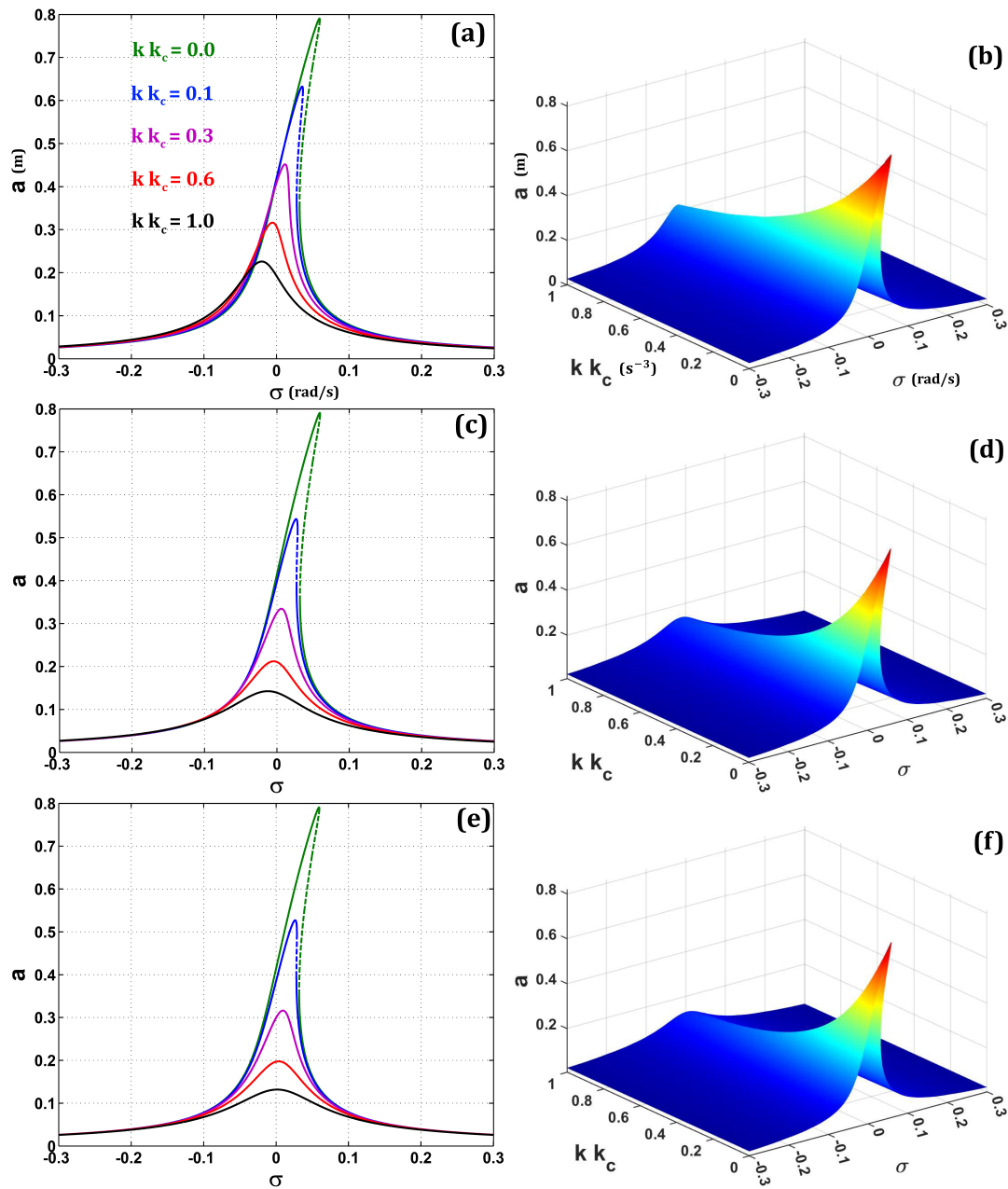
Figure 11: Response of the car's motion amplitude a to the frequency detuning σ and the gain product kk_c: (a, b) $\omega_c = \omega$, (c, d) $\omega_c = 1$, (e, f) $\omega_c = 0$
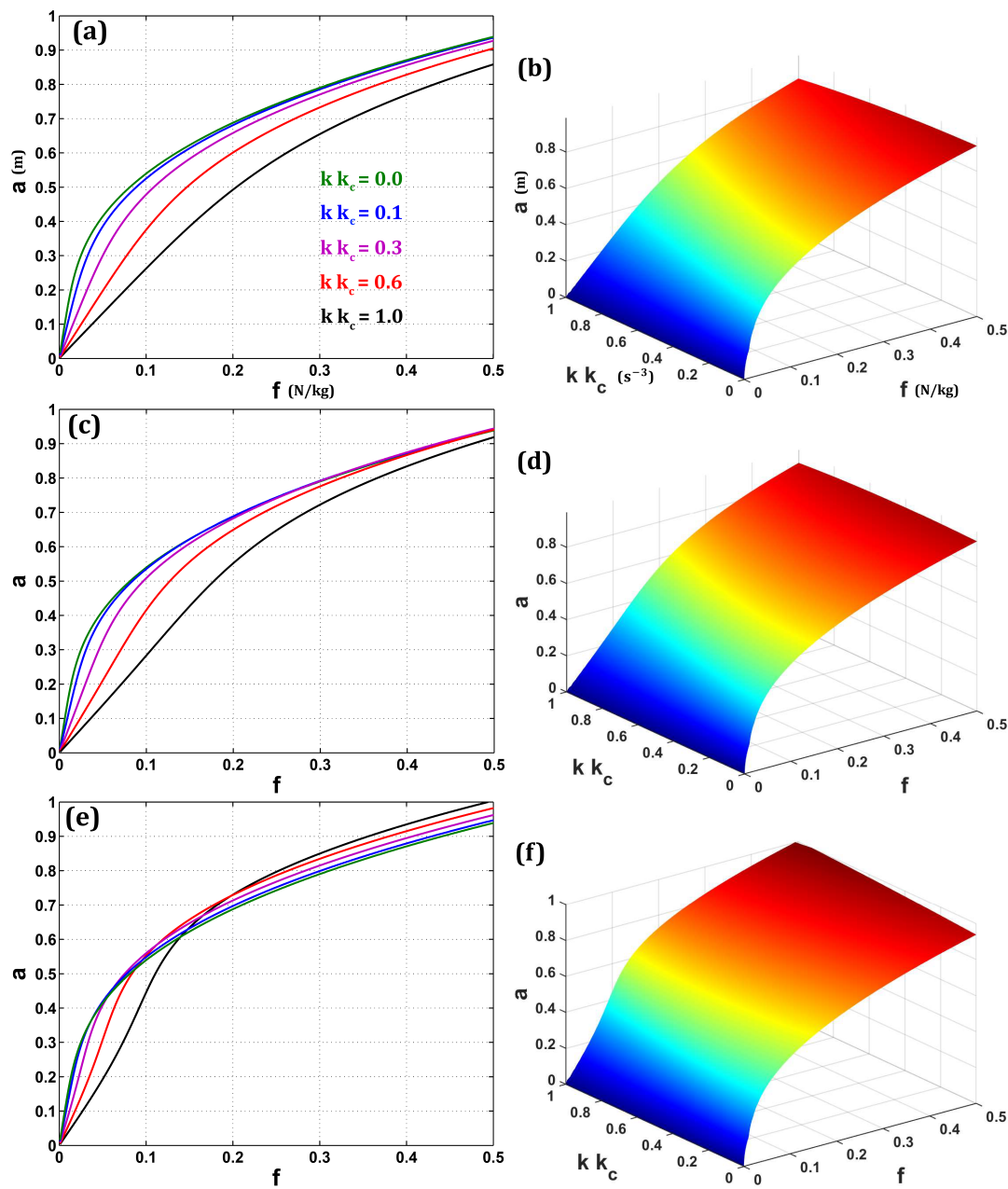
Figure 12: Response of the car's motion amplitude a to the force amplitude f and the gain product kk_c at $\sigma = 0$: (a, b) $\omega_c = 0$, (c, d) $\omega_c = 1$, (e, f) $\omega_c = \omega$
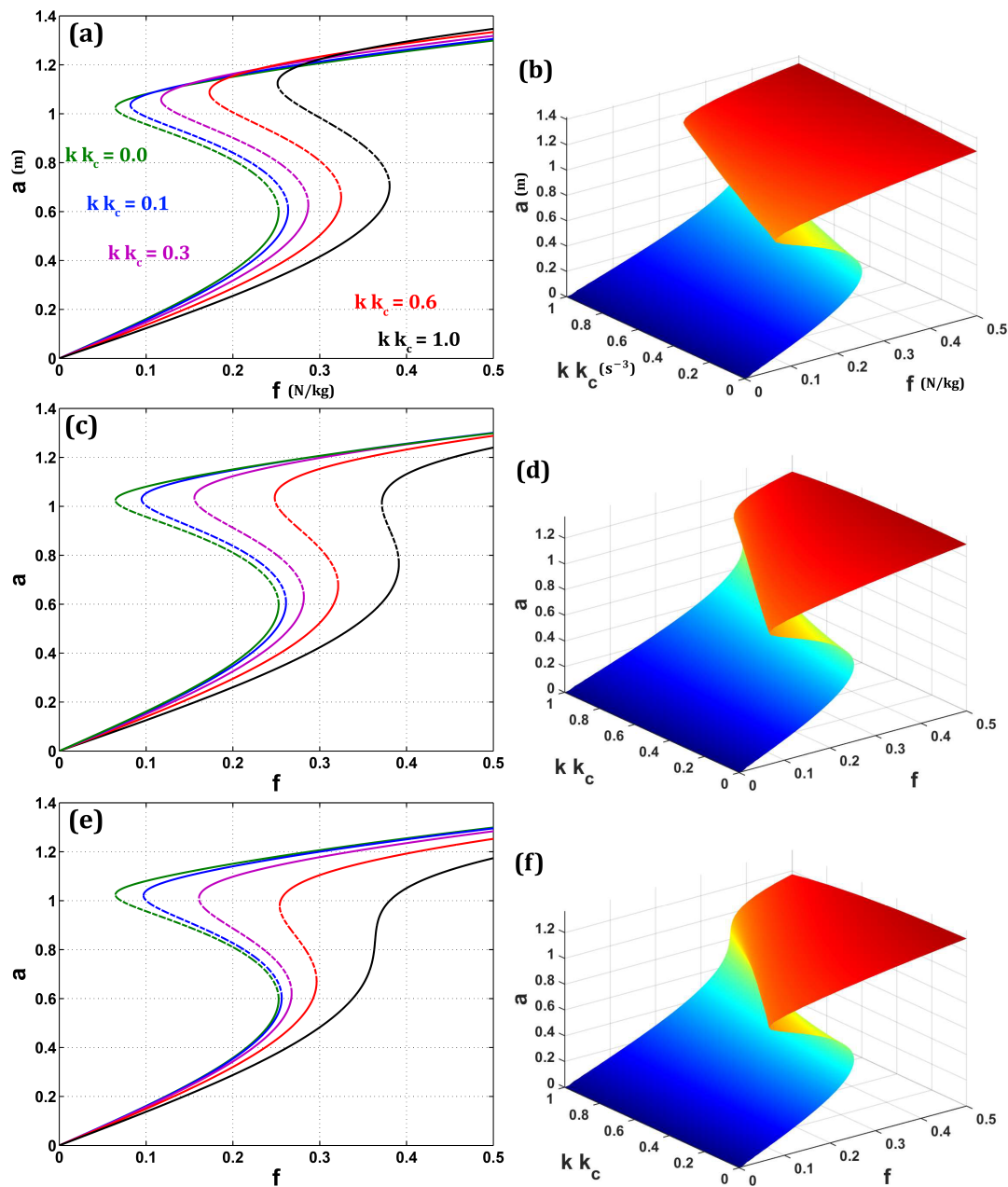
Figure 13: Response of the car's motion amplitude a to the force amplitude f and the gain product kk_c at $\sigma = 0.1$: (a, b) $\omega_c = \omega$, (c, d) $\omega_c = 1$, (e, f) $\omega_c = 0$

4. Numerical Simulation of The Car's Motion

Regarding the numerical simulation of the car's motion, the fourth-order Runge-Kutta technique has been adopted in order to integrate Eqs. (3) and (4) numerically. The resulting time responses are plotted to verify the analytical approximate responses that

were discussed earlier in Figs. 2 to 13. Figures 14 and 15 describe the time response evolution of the car's amplitude through transient and steady-state cases as shown. We have adopted the same parameters values discussed previously except for the value of ω_c which had a zero value (theoretically) but has the value 0.1 for stable practical operation as will be shown. Equations (3) and (4) can be reformulated in the sense of autonomous system by assuming the new variables $u = \cos(\Omega t)$ and $v = \sin(\Omega t)$ as follows:

$$\ddot{x} + \mu\dot{x} + \omega^2 x + \alpha x^3 = fu + ky \tag{30}$$

$$\dot{y} + \omega_c y = k_c x \tag{31}$$

$$\dot{u} = -\Omega v \tag{32}$$

$$\dot{v} = \Omega u \tag{33}$$

Linearizing the system of equations above along with assuming that $x = x_1$ and $\dot{x} = x_2$, then rewriting the system in the state-space matrix form as follows:

$$\begin{bmatrix} \dot{x}_1 \\ \dot{x}_2 \\ \dot{y} \\ \dot{u} \\ \dot{v} \end{bmatrix} = \begin{bmatrix} 0 & 1 & 0 & 0 & 0 \\ -\omega^2 & -\mu & k & f & 0 \\ k_c & 0 & -\omega_c & 0 & 0 \\ 0 & 0 & 0 & 0 & -\Omega \\ 0 & 0 & 0 & \Omega & 0 \end{bmatrix} \begin{bmatrix} x_1 \\ x_2 \\ y \\ u \\ v \end{bmatrix} \tag{34}$$

Applying the Routh-Hurwitz technique on the square matrix above gives us some conditions for the system to be stable. These conditions give us that ω_c should obey the inequality $(\omega_c \omega^2 - kk_c) \geq 0$. Based on the last criterion, ω_c can have the minimum value 0.1 if the product $kk_c = 1.0$ and $\omega^2 = 10$. This optimum value of ω_c is proved for the practical operation of the car not to make any confusion with the theoretical approach we have discussed before. Figure 14 shows the time response of the car's maximum displacement in case that $f = 0.06$ and IRC is OFF ($k = 0$) then ON ($kk_c = 1$ and $\omega_c = 0.1$) at different values of σ. It can be seen that the car's peak displacement x_p is about 0.44 at $\sigma = 0$ (Fig. 14a) during forward sweeping until σ reaches 0.065 where x_p is about 0.85 then suddenly x_p jumps down to about 0.15 at $\sigma = 0.070$ (Fig. 14b). In the backward sweeping process, the car's peak displacement x_p is about 0.2 at $\sigma = 0.050$ (Fig. 14c) until σ reaches 0.045 where x_p jumps up suddenly to about 0.75 (Fig. 14c). The proposed control algorithm will treat such severe jumps. In Fig. 14a where $\sigma = 0$, the controlled car's peak displacement has been suppressed by about 64% of its uncontrolled value. In Figs. 14b and 14c, the jump phenomena have been eliminated as shown and the controlled car's peak displacement has become lower than the lower amplitude before control. Moreover, Fig. 15 indicates the time history of the car's maximum displacement in case that $\sigma = 0.1$ and IRC is OFF ($k = 0$) then ON ($kk_c = 1$ and $\omega_c = 0.1$) for different values of f. One can see that the car's peak displacement x_p is about 0.095 at $f = 0.06$ (Fig. 15a). During forward sweeping in Fig. 15b, the force f reaches 0.15 where x_p is about 0.34 then a sudden jump-up happens in x_p to about 1.15 at $f = 0.16$. During backward sweeping in Fig. 15c, the car's peak displacement x_p is about 1.1 at $f = 0.10$ until f reaches 0.09 where x_p jumps down suddenly to about 0.15. Again, the proposed control algorithm has

treated the issue of the jump phenomena as shown in Fig. 15 where x_p is reduced by about 16% of its uncontrolled state. Figures 15b and c show the elimination of the jump phenomena in addition that x_p went lower than the uncontrolled lower amplitude.
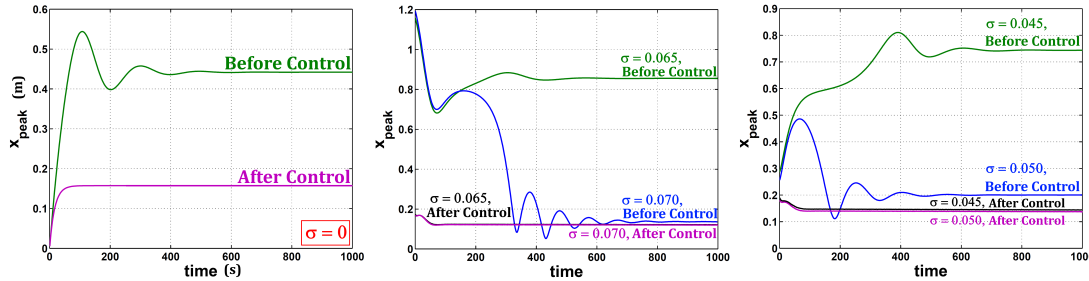

Figure 14: Response of the car's maximum displacement to the time t in case that $f = 0.06$ and IRC is OFF ($k = 0$) then ON ($kk_c = 1$ and $\omega_c = 0.1$): (left) $\sigma = 0$, (middle) forward sweeping of $\sigma = 0.065, 0.070$, (right) backward sweeping of $\sigma = 0.050, 0.045$
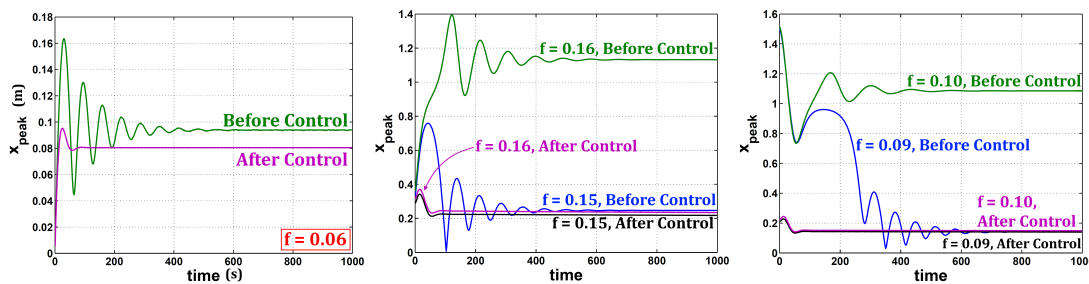

Figure 15: Response of the car's maximum displacement to the time t in case that $\sigma = 0.1$ and IRC is OFF ($k = 0$) then ON ($kk_c = 1$ and $\omega_c = 0.1$): (left) $f = 0.06$, (middle) forward sweeping of $f = 0.15, 0.16$, (right) backward sweeping of $f = 0.10, 0.09$

5. Concluding Remarks

In this paper, a horizontally-supported car's motion has been modeled under the effect of a nonlinear spring, a damper, and a harmonic excitation external force. The car's oscillations were controlled via an integral resonant controller whose operation was built on a linear variable differential transformer and a servo-controlled linear actuator. The multiple scales perturbation technique was adopted to seek an approximate solution of the proposed nonlinear system of equations. In addition, a stability analysis was achieved in order to determine whether the extracted approximate solution was stable or unstable. Several response curves were plotted for clarifying the concept of the proposed control algorithm. Regarding the numerical simulation of the car's motion, the Runge-Kutta technique was used in order to integrate the model equations numerically. Based upon the gained results of this work, we have concluded some summarized remarks. The car's damping behavior could be enhanced by adjusting the control rate ω_c to be zero (theoretically). In addition, this performance could be also enhanced by raising the product kk_c to 1.0 which was an acceptable value for guaranteeing a better damping performance.

Another advantage appeared at the optimum values of kk_c and ω_c which was the elimination of the jump phenomena and the unstable regions of the response curves (frequency or force response curves). Based on a stability analysis of the original model equations, the control rate ω_c should have the minimum value 0.1 (practically) if the product $kk_c = 1.0$ and $\omega^2 = 10$. The proposed control algorithm treated the car's amplitude severe jumps where it was being suppressed at different conditions of forward and backward sweeping of the parameters σ and f.

Acknowledgements

Declaration of Conflicting Interests

The authors declared no potential conflicts of interest with respect to the research, authorship, and/or publication of this article.

References

[1] Abdullah Al-Mamun, Ehsan Keikha, Charanjit Singh Bhatia, and Tong Heng Lee. Integral resonant control for suppression of resonance in piezoelectric micro-actuator used in precision servomechanism. *Mechatronics*, 23(1):1–9, 2013.

[2] Sumeet S Aphale, Andrew J Fleming, and SO Reza Moheimani. Integral resonant control of collocated smart structures. *Smart materials and structures*, 16(2):439, 2007.

[3] Hany Bauomy and Ashraf Taha. Nonlinear saturation controller simulation for reducing the high vibrations of a dynamical system. *Math. Biosci. Eng*, 19:3487–3508, 2022.

[4] Klaas B Bronkhorst, Mariano Febbo, Eduardo MO Lopes, and Carlos A Bavastri. Experimental implementation of an optimum viscoelastic vibration absorber for cubic nonlinear systems. *Engineering Structures*, 163:323–331, 2018.

[5] Ivan M Diaz, Emiliano Pereira, and Paul Reynolds. Integral resonant control scheme for cancelling human-induced vibrations in light-weight pedestrian structures. *Structural Control and Health Monitoring*, 19(1):55–69, 2012.

[6] Iván M Díaz and Paul Reynolds. Robust saturated control of human-induced floor vibrations via a proof-mass actuator. *Smart Materials and Structures*, 18(12):125024, 2009.

[7] Mariano Febbo. Harmonic response of a class of finite extensibility nonlinear oscillators. *Physica Scripta*, 83(6):065009, 2011.

[8] Mariano Febbo and Jinchen Ji. On the critical forcing amplitude of forced nonlinear oscillators. *Open Engineering*, 3(4):764–770, 2013.

[9] Xiaofeng Geng, Hu Ding, Xingjian Jing, Xiaoye Mao, Kexiang Wei, and Liqun Chen. Dynamic design of a magnetic-enhanced nonlinear energy sink. *Mechanical Systems and Signal Processing*, 185:109813, 2023.

[10] J. C. Ji. Application of a weakly nonlinear absorber to suppress the resonant vibrations of a forced nonlinear oscillator. *Journal of Vibration and Acoustics*, 134(4):044502, 2012.

[11] JC Ji and N Zhang. Suppression of the primary resonance vibrations of a forced nonlinear system using a dynamic vibration absorber. *Journal of Sound and Vibration*, 329(11):2044–2056, 2010.

[12] Ali Kandil, Yasser S Hamed, Khadijah M Abualnaja, Jan Awrejcewicz, and Maksymilian Bednarek. 1/3 order subharmonic resonance control of a mass-damper-spring model via cubic-position negative-velocity feedback. *Symmetry*, 14(4):685, 2022.

[13] Ali Kandil, Yasser S Hamed, Mohamed S Mohamed, Jan Awrejcewicz, and Maksymilian Bednarek. Third-order superharmonic resonance analysis and control in a nonlinear dynamical system. *Mathematics*, 10(8):1282, 2022.

[14] Ali Kandil, Yasser Salah Hamed, Abdullah M Alsharif, and Jan Awrejcewicz. 2d and 3d visualizations of the mass-damper-spring model dynamics controlled by a servo-controlled linear actuator. *IEEE Access*, 9:153012–153026, 2021.

[15] Ali Kandil, YS Hamed, and Jan Awrejcewicz. Harmonic balance method to analyze the steady-state response of a controlled mass-damper-spring model. *Symmetry*, 14(6):1247, 2022.

[16] Canchang Liu, Chuanbo Ren, Lu Liu, and Yingzi Xu. Optimal control of nonlinear vibration resonances of single-walled nanotube beams. *Acta Mechanica Solida Sinica*, 27(6):648–656, 2014.

[17] Canchang Liu, Shuchang Yue, and Jilei Zhou. Piezoelectric optimal delayed feedback control for nonlinear vibration of beams. *Journal of Low Frequency Noise, Vibration and Active Control*, 35(1):25–38, 2016.

[18] Chun-Xia Liu, Yan Yan, and Wen-Quan Wang. Primary and secondary resonance analyses of a cantilever beam carrying an intermediate lumped mass with time-delay feedback. *Nonlinear Dynamics*, 97:1175–1195, 2019.

[19] Chunxia Liu, Yan Yan, and Wen-Quan Wang. Application of nonlocal continuum theory to the primary resonance analysis of an axially loaded nano beam under time delay control. *Applied Mathematical Modelling*, 85:124–140, 2020.

[20] Chunxia Liu, Yan Yan, Wenquan Wang, and Daohang Wang. Optimal time delayed control of the combination resonances of viscoelastic graphene sheets under dual-frequency excitation. *Chaos, Solitons & Fractals*, 165:112856, 2022.

[21] WB Liu, HL Dai, and L Wang. Suppressing wind-induced oscillations of prismatic structures by dynamic vibration absorbers. *International Journal of Structural Stability and Dynamics*, 17(06):1750056, 2017.

[22] S Mohanty and SK Dwivedy. Traditional and non-traditional active nonlinear vibration absorber with time delay combination feedback for hard excitation. *Communications in Nonlinear Science and Numerical Simulation*, 117:106919, 2023.

[23] Ali H Nayfeh and Dean T Mook. *Nonlinear oscillations*. John Wiley & Sons, 2008.

[24] Ehsan Omidi and S Nima Mahmoodi. Sensitivity analysis of the nonlinear integral positive position feedback and integral resonant controllers on vibration suppression of nonlinear oscillatory systems. *Communications in Nonlinear Science and Numerical Simulation*, 22(1-3):149–166, 2015.

[25] Ehsan Omidi and S Nima Mahmoodi. Nonlinear integral resonant controller for vibration reduction in nonlinear systems. *Acta Mechanica Sinica*, 32:925–934, 2016.

[26] Hasan Omur Ozer, Yuksel Hacioglu, and Nurkan Yagiz. Suppression of structural vibrations using pdpi+ pi type fuzzy logic controlled active dynamic absorber. *Journal of the Brazilian Society of Mechanical Sciences and Engineering*, 38:2105–2115, 2016.

[27] Emiliano Pereira, Sumeet S Aphale, Vicente Feliu, and SO Reza Moheimani. Integral resonant control for vibration damping and precise tip-positioning of a single-link flexible manipulator. *IEEE/ASME Transactions on Mechatronics*, 16(2):232–240, 2010.

[28] Nasser A Saeed, Mohamed S Mohamed, Sayed K Elagan, and Jan Awrejcewicz. Integral resonant controller to suppress the nonlinear oscillations of a two-degree-of-freedom rotor active magnetic bearing system. *Processes*, 10(2):271, 2022.

[29] Jean-Jacques E Slotine, Weiping Li, et al. *Applied nonlinear control*. Prentice hall Englewood Cliffs, NJ, 1991.

[30] Feng Wang, Xiuting Sun, Hao Meng, and Jian Xu. Tunable broadband low-frequency band gap of multiple-layer metastructure induced by time-delayed vibration absorbers. *Nonlinear Dynamics*, pages 1–16, 2022.

[31] Jian Xu and Xiuting Sun. A multi-directional vibration isolator based on quasi-zero-stiffness structure and time-delayed active control. *International Journal of Mechanical Sciences*, 100:126–135, 2015.

[32] Tiancheng Xu, Yancheng Li, Tao Lai, and Shaoqi Li. h_2 and h_∞ optimal designs of tuned inerter dampers for base motion excited structures with inherent damping. *Journal of Vibration and Control*, 29(15-16):3692–3707, 2023.

[33] Wei-Xing Zhang, Wei Zhang, Dong-Shuo Yang, Zhong Luo, and Xiang-Ying Guo. Vibration suppression of nonlinear laminated composite plates using internal oscillator-enhanced nonlinear energy sinks. *Engineering Structures*, 279:115579, 2023.

[34] J Zhou, W Zhang, XS Wang, BP Mann, and EH Dowell. Primary resonance suppression of a base excited oscillator using a spatially constrained system: Theory and experiment. *Journal of Sound and Vibration*, 496:115928, 2021.